Physica B 532 (2018) 139–143

Contents lists available at ScienceDirect

Physica B

journal homepage: www.elsevier.com/locate/physb

Phase transitions in the Haldane-Hubbard model within coherent potential approximation

Duc-Anh Le[a,*], Minh-Tien Tran[b,c,d], Thi-Thanh-Mai Tran[a], Thi-Thao Nguyen[a], Thi-Huong Nguyen[e], Anh-Tuan Hoang[d]

[a] Faculty of Physics, Hanoi National University of Education, Xuan Thuy 136, Cau Giay, Hanoi 10000, Vietnam
[b] Institute of Research and Development, Duy Tan University, K7/25 Quang Trung, Danang, Vietnam
[c] Graduate University of Science and Technology, Vietnam Academy of Science and Technology, 18 Hoang Quoc Viet, Cau Giay, Hanoi, Vietnam
[d] Institute of Physics, Vietnam Academy of Science and Technology, 10 Dao Tan, Hanoi, Vietnam
[e] Water Resources University, Tay Son 175, Dong Da, Hanoi 10000, Viet Nam

ARTICLE INFO

Keywords:
Haldane-Hubbard model
Topological states
Metal-insulator transitions

ABSTRACT

Within the coherent potential approximation we study the two-dimensional Haldane-Hubbard model, in which an interplay between topology and correlation effects is realized. The model essentially describes correlated electrons moving in a honeycomb lattice with zero net magnetic flux. The influence of the next-nearest-neighbor hopping and electron correlations on the metal-insulator transitions are investigated by monitoring the density of states at the Fermi level and the energy gap. The topological properties of the insulators is determined by the Chern number. With a given next-nearest-neighbor hopping, electron correlations drive the system from the topological Chern insulator to a metal, and then to the topologically trivial Mott insulator.

1. Introduction

Recently, two dimensional honeycomb structure of atoms has been extensively studied because its properties are of big importance in the realm of science [1,2]. The already obtained outcome from these important first steps in understanding the two dimensional materials showed promising features that could give a new future to silicon in the electronics industry, thus opening a promising route toward wide-range applications [3]. Very recently, silicene has been made transistor debut [4]. This is a significant step towards in realizing silicene application. The effect when silicene is grown on a substrate such as Ag (111) as suggested by line-profile scanning tunneling microscopy measurements [2,5], can be explored using an ionic potential that may remove the linear Dirac fermion nature of the energy bands near the Dirac points [6]. In two dimensional materials like graphene or silicene, when the magnetic field perpendicularly penetrates the lattice, the quantum Hall effect (QHE) occurs. The QHE is essentially a topological state, which is distinct from standard symmetry-breaking states. It is interesting to seek materials which exhibit topological ground state in the absence of the external magnetic field. In his seminal paper, Haldane proposed a lattice model, in which the ground state is topological, but the net lattice magnetic flux is zero [7]. The Haldane model is essentially a tight-binding model of spinless electrons moving on a honeycomb lattice. It is the first lattice model which exhibits the topological properties. Since the two-dimensional materials like graphene or silicence have the same lattice structure as the Haldane model, one may seek the conditions at which these materials may exhibit topological properties. Recently, the Haldane model has been experimentally realized by loading ultracold fermionic atoms in an optical honeycomb lattice, and its ground state is verified to be topological [8,9]. In real materials electron correlations often play an important role in the physical properties. However, they are absent in the Haldane model. It is interesting to study the interplay between topological properties and electron correlations in two-dimensional systems. The interplay can be realized by combining the Haldane model and the Coulomb interaction between electrons. Most studies have introduced nonlocal nearest neighbor Coulomb repulsion into the Haldane model to investigate its effects on the topological properties [10,11]. The nonlocal Coulomb interactions drive the system into topologically trivial charge-ordered insulator and the transition is of first order [10,11]. However, the nonlocal interaction is often weaker than the local one. The latter has been also introduced into the Haldane model with an ionic potential [12] or without an ionic potential [13–17] to study the local correlation-driven phase transition in the Chern insulator. When the ionic potential is present, Vanhala *et al.* has found a spontaneous symmetry breaking quantum Hall phase, where one of the spin components is in the Hall state and the other in the band insulating state [12]. When the ionic potential is

* Corresponding author.
E-mail address: anhld@hnue.edu.vn (D.-A. Le).

http://dx.doi.org/10.1016/j.physb.2017.06.084
Received 21 December 2016; Received in revised form 14 May 2017; Accepted 29 June 2017
Available online 30 June 2017
0921-4526/

not present, it is established that Chern insulator (CI) is stable against the Hubbard interaction for $U < U_C$, where the value of U_C depends on the approach being used. However, different approaches lead to different results regarding what phases are stable for $U > U_C$, and in what order. Calculations based on the mean-field theories and beyond suggested that the stable state at large U is the antiferromagnetic state [13–17]. However, these studies still provide different conclusion for intermediate U.

In this paper, we consider the Haldane-Hubbard model on a honeycomb lattice when the local interaction U is intermediate and the ionic potential is absent. We employ the coherent potential approximation (CPA), which is a successful theory for the Hubbard model on a honeycomb lattice [6,18]. We investigate the influence of the next-nearest-neighbor hopping and electron correlation on the metal-insulator transitions by monitoring the density of states at the Fermi level and the energy gap. The topological properties of the insulators is obtained by the Chern number and the phase diagram is numerically contracted. This paper is organized as follows. The Haldane-Hubbard model and the coherent potential approximation are presented in the next section. In Section 3 we discuss our numerical results. Finally, the paper is concluded and the directions of future work are in Section 4.

2. Model and formalism

We consider a hybrid of the spin version of the Haldane and Hubbard models, in which spin-1/2 fermions hop on a lattice according to Haldane's original tight-binding model, also when two fermions of opposite spin projection are at the same site they repel each other with the potential energy U. On a honeycomb lattice, the Hamiltonian reads

$$H= -t\sum_{\langle i,j\rangle,\sigma}[c^{+}_{i\sigma}c_{j\sigma}+H.\,c]+U\sum_{i}n_{i\uparrow}n_{i\downarrow} -\mu\sum_{i}n_{i}+\lambda\sum_{\langle\langle i,j\rangle\rangle,\sigma}\nu_{ij}c^{+}_{i\sigma}c_{j\sigma}. \quad (1)$$

Here $c^{+}_{i\sigma}(c_{i\sigma})$ is the creation (annihilation) operator for electron with spin σ at site i, $n_{i\sigma}=c^{+}_{i\sigma}c_{i\sigma}$ and $n_i=n_{i\uparrow}+n_{i\downarrow}$. t is the hopping parameter for the nearest neighbor sites. U is the on-site Coulomb repulsion. $\langle i,j\rangle$ and $\langle\langle i,j\rangle\rangle$ denote the nearest neighbor and next nearest neighbor sites in the lattice, respectively. λ is the hopping parameter between next nearest neighbor sites. Parameter $\nu_{ij}=exp(i\Phi_{ij})$ describes the phase of electrons attained when electrons hop from lattice site i to site j in the presence of a staggered magnetic flux perpendicularly penetrating the lattice. Since the honeycomb lattice is bipartite, the penetrating magnetic flux in each sublattice has opposite value, the total net magnetic flux is zero. Notice that the staggered magnetic flux does not affect the nearest neighbor hopping, since the magnetic flux per one hexagonal unit is zero. When U=0 the proposed model is just the spin version of the Haldane model. Its ground state is topological except for $\Phi_{ij}=0,\ \pi$ [7]. Without loss of generality, in this paper we consider only the case $\Phi_{ij}=\pm\frac{\pi}{2}$, at which the ground state of the Haldane model is topological. Therefore, $\nu_{ij}=\pm i$ depends on the hopping direction (clockwise or anticlockwise) as shown in Fig. 1. The chemical potential $\mu=U/2$ so that the average occupancy is 1 (half-filling). When $\lambda=0$, the Hamiltonian in Eq. (1) is just the standard Hubbard model on a bipartite lattice, which exhibits the metal-insulator transition for the homogeneous states, where the inversion symmetry is preserved. In the other limit, when $t=0$, the model described in Eq. (1) is equivalent to two independent triangular lattices of the Hubbard model. The triangular lattice is geometrically frustrated; thus, we expect the homogeneous states are stable at low temperatures. The Haldane-Hubbard model under consideration breaks time-reversal symmetry, which leads to the notorious fermion sign problem and precludes the use of methods based on the quantum Monte-Carlo algorithm. In this study, we do not consider large values of λ for which topological spin

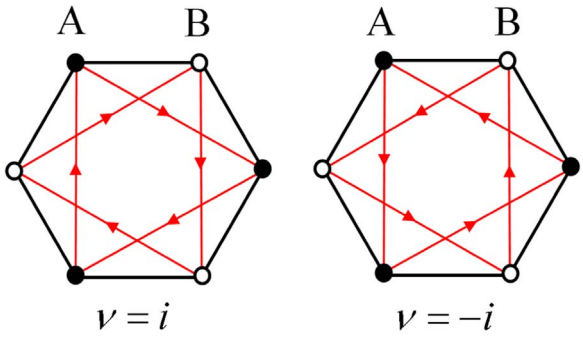

Fig. 1. The sign structure of the next nearest neighbor hopping term in the honeycomb lattice.

density waves, chiral topological orders, and exotic kinds of magnetic order have been suggested [19–21]. Also, we will consider only the repulsive local interaction so that it does not support topological superfluids to appear [22].

In the alloy-analogue approach, the many-body Hamiltonian (1) is replaced by a one-particle Hamiltonian with disorder which is of the form

$$H= -t\sum_{\langle i,j\rangle,\sigma}[c^{+}_{i\sigma}c_{j\sigma}+H.\,c]+\sum_{i\in A,\sigma}E_{A\sigma}n_{i\sigma} +\sum_{i\in B,\sigma}E_{B\sigma}n_{i\sigma}+\lambda\sum_{\langle\langle i,j\rangle\rangle,\sigma}exp(i\Phi_{ij})c^{+}_{i\sigma}c_{j\sigma}. \quad (2)$$

Here the disorder potential has been defined to include the chemical potential, which is given by

$$E_{\alpha,\sigma}=\begin{cases}-\mu & \text{with probability}\quad 1-n_{\alpha\bar{\sigma}},\\ -\mu+U & \text{with probability}\quad n_{\alpha\bar{\sigma}},\end{cases}$$

where, α = A, B and $n_{\alpha\bar{\sigma}}$ is the average occupation for spin $\bar{\sigma}$ in the α-sublattice. The Green function of the Hamiltonian (2) has to be averaged over all possible configurations of the random potential, which can be considered to be due to alloy constituents. The averaging cannot be performed exactly. To deal with this problem, we use the CPA that introduces a simplified effective medium corresponding to a local ($\vec{k}$ independent) complex and energy-dependent single-site self-energy or coherent potential $\Sigma_{\alpha\sigma}$ that replaces $E_{\alpha\sigma}$ on each sublattice α = A, B in Hamiltonian (2)

$$H_{eff}= -t\sum_{\substack{\langle i,j\rangle,\sigma\\ i\in A,j\in B}}[c^{+}_{i\sigma}c_{j\sigma}+H.\,c]+\sum_{i\in A,\sigma}\Sigma_{A\sigma}n_{i\sigma} +\sum_{j\in B,\sigma}\Sigma_{B\sigma}n_{j\sigma}+\lambda\sum_{\langle\langle i,j\rangle\rangle,\sigma}exp(i\Phi_{ij})c^{+}_{i\sigma}c_{j\sigma}. \quad (3)$$

It is straightforward to obtain the lattice Green function

$$F_{A\uparrow}(\omega)=\frac{1}{\Omega}\sum_{\vec{k}}\frac{\omega-\Sigma_{B\uparrow}+\lambda\xi_{\vec{k}}}{(\omega-\Sigma_{A\uparrow}-\lambda\xi_{\vec{k}})(\omega-\Sigma_{B\uparrow}+\lambda\xi_{\vec{k}})-t^2|\gamma_{\vec{k}}|^2},$$

$$F_{B\uparrow}(\omega)=\frac{1}{\Omega}\sum_{\vec{k}}\frac{\omega-\Sigma_{A\uparrow}-\lambda\xi_{\vec{k}}}{(\omega-\Sigma_{A\uparrow}-\lambda\xi_{\vec{k}})(\omega-\Sigma_{B\uparrow}+\lambda\xi_{\vec{k}})-t^2|\gamma_{\vec{k}}|^2},$$

$$F_{A\downarrow}(\omega)=\frac{1}{\Omega}\sum_{\vec{k}}\frac{\omega-\Sigma_{B\downarrow}+\lambda\xi_{\vec{k}}}{(\omega-\Sigma_{A\downarrow}-\lambda\xi_{\vec{k}})(\omega-\Sigma_{B\downarrow}+\lambda\xi_{\vec{k}})-t^2|\gamma_{\vec{k}}|^2},$$

$$F_{B\downarrow}(\omega)=\frac{1}{\Omega}\sum_{\vec{k}}\frac{\omega-\Sigma_{A\downarrow}-\lambda\xi_{\vec{k}}}{(\omega-\Sigma_{A\downarrow}-\lambda\xi_{\vec{k}})(\omega-\Sigma_{B\downarrow}+\lambda\xi_{\vec{k}})-t^2|\gamma_{\vec{k}}|^2},$$

where the integral is over the first Brillouin zone with the volume Ω.

Here we have used the notations $\gamma_{\vec{k}}=\sum_{\vec{R}}e^{i\vec{k}\vec{R}}$, $\xi_{\vec{k}}=i\sum_{\vec{\delta}}\nu_{\delta}e^{i\vec{k}\vec{\delta}}$, with $\vec{R}$ is the nearest-neighbor vector and $\vec{\delta}$ is the next nearest-neighbor vector in the honeycomb lattice.

The self-consistent condition of the CPA requires that the lattice Green function must coincide with the conditional Green function, i.e.,

$$F_{\alpha\sigma}(\omega) = G_{\alpha\sigma}(\omega), \tag{4}$$

where the conditional Green function is determined for each α-sublattice as follows

$$G_{\alpha\sigma}(\omega) = \frac{F_{\alpha\sigma}(\omega)(1 - n_{\alpha\bar{\sigma}})}{1 + F_{\alpha\sigma}(\omega)(\Sigma_{\alpha\sigma}(\omega) + \mu)} + \frac{F_{\alpha\sigma}(\omega)n_{\alpha\bar{\sigma}}}{1 + F_{\alpha\sigma}(\omega)(\Sigma_{\alpha\sigma}(\omega) + \mu - U)}. \tag{5}$$

So far, for determining the Green function we have obtained a closed system of equations, which can be solved numerically by simple iterations.

3. Results and discussions

We solve numerically the self-consistent equations (4)–(5) to determine the self-energy and the Green function by simple iterations. The algorithm is similar to that presented in Ref. [18] as follows. Begin with an initial self-energy guess for all frequencies $\Sigma_{\alpha\sigma}(\omega)$, one obtains the frequency dependent Green function $F_{\alpha\sigma}(\omega)$ by taking the summation over $\vec{k}$ in the first Brillouin zone. Substituting the self-energy $\Sigma_{\alpha\sigma}(\omega)$ and the lattice Green function $F_{\alpha\sigma}(\omega)$ were calculated in the previous step to Eq. (5) one calculates the conditional Green function $G_{\alpha\sigma}(\omega)$. Finally, a new self energy $\Sigma_{\alpha\sigma}(\omega)$ is determined by

$$\Sigma_{\alpha\sigma}(\omega) = \Sigma_{\alpha\sigma}(\omega) + \frac{1}{F_{\alpha\sigma}(\omega)} - \frac{1}{G_{\alpha\sigma}(\omega)}, \tag{6}$$

which is equivalent to Eq. (4). This procedure is iterated until convergence is reached. In actual numerical calculations, an analytical continuation $\omega \to \omega + i\eta$ needs to be performed, where η is a positive infinitesimal number. In numerical calculations, we take t=1 as the energy unit, therefore η should be a finite small one in a range from 10^{-3} to 10^{-2} to make the iterations converges. The smaller η, the more computational CPU time is required. If η is too small, the convergence is even never reached. The effect due to finite η is to broaden the density of states when the self-energy $\Sigma_{\alpha\sigma}(\omega)$ is real. This effect can be neglected if the imaginary part of the self-energy is large enough. When the transition point is approached, the effect causes a small artificial peak at the Fermi level. In order to obtain a sharp picture for the density of states, which is particularly important to determine the critical value U_C for the semimetal-insulator transition, we use the spline extrapolation to reach the $\eta \to 0$ limit.

We have done the numerical calculations for a number of values of the next nearest neighbor hopping λ and the local interaction strength U. It turns out that the groundstate is a homogeneous paramagnetic, i.e., $n_{A\uparrow} = n_{A\downarrow} = n_{B\uparrow} = n_{B\downarrow} = \frac{1}{2}$. In the noninteracting limit $U \to 0$, the problem can be solved exactly. This results is crucial since it will shed the light for the numerical calculation for intermediate interaction strength U. Therefore, in the following, we will firstly discuss the results for the case U=0 and then the results for finite U.

When U=0, the $\vec{k}$-dependent energy spectra reads $E_{\pm\sigma}(\vec{k}) = \pm\frac{1}{2}\sqrt{(2\lambda\xi_{\vec{k}})^2 + 4t^2\gamma_{\vec{k}}^2}$. Because $\gamma_{\vec{k}}$ and $\xi_{\vec{k}}$ are spin independent, the degeneracy of upper and lower bands is 2. The energy gap can be easily determined by minimum of $\sqrt{(2\lambda\xi_{\vec{k}})^2 + 4t^2\gamma_{\vec{k}}^2}$. If $\lambda = 0$, the system is semimetal with pseudogap is 0 since the two bands touching at the $K(\frac{2\Pi}{3a}, \frac{2\Pi}{3\sqrt{3}a})$ point of the hexagonal Brillouin zone, where a is the lattice constant of the honeycomb lattice. For intermediate λ, the two bands are separated resulting in an insulating state of the system. When $0 < \lambda \leq \sqrt{3}/9$, the gap of the system is found at the K point that equals to $6\sqrt{3}\lambda$. In contrast, when $\lambda > \sqrt{3}/9$, the gap equals 2 is found at the $M(\frac{2\Pi}{3a}, \frac{2\Pi}{3\sqrt{3}a})$ point, which is independent of λ. The exact values of the gap in the noninteracting limit will be used to check the numerical calculations for the gap for the intermediate values of the local interaction U.

Now, for a given value of λ, we will increase the local interaction U. The results for different value of λ is qualitatively the same but quantitatively different. When the local interaction is small enough, $U < U_{C1}$ the system is a topologically nontrivial band insulator. If U is intermediate, $U_{C1} < U < U_{C2}$ the system is metallic. For large enough U, $U > U_{C2}$, the strong local correlation drives the system into a topologically trivial Mott insulator.

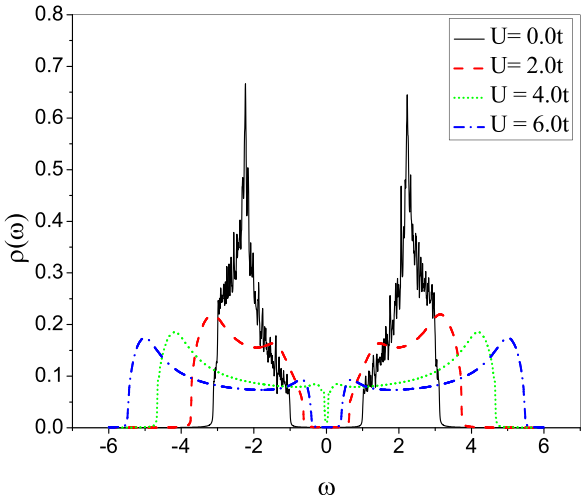

Fig. 2. The density of states for various values of U (t=1, λ=0.2).

In the following, we will discuss results for $\lambda = 0.2$ in detail. Fig. 2 presents the density of states (DOS) for various values of U. Fig. 3 shows the DOS at the Fermi level as a function of the onsite Coulomb interaction U. When U increases, it appears two transitions. Firstly, the correlations drive the system from band insulator phase to metallic phase, then from metallic phase to Mott insulator phase. By extrapolating the density of states at the Fermi level for the metallic state, $3.0 < U/t < 3.7$ as showed in Fig. 3, we obtain that metallic phase vanished at $U_{C1} \approx 2.75t$ and $U_{C2} \approx 3.8t$, respectively. However, since the DOS at the Fermi level is quite small, it is better to determine the transition points from the gap data in the insulating phase. Fig. 4 presents the insulating gap as a function of the onsite Coulomb repulsion, where the numerical results are plotted by filled cycles and the solid line is obtained by the spline method. In order to calculate the gap, one can introduce a small fictitious temperature and find the chemical potential $\mu_{\pm}$ for the filling $n = 1 \pm \epsilon$. The small positive ϵ is chosen so that the numerically calculated gap $\mu_+ - \mu_-$ is in good agreement with the known results in the noninteracting case U=0 as discussed above. By extrapolating the data for $U/t < 2.5$ and $U/t > 4$, we obtain that the gap is vanished $U_{C1} \approx 2.83t$ and $U_{C2} \approx 3.88t$. If one could reduce the values of the positive number η in the analytical continuation $\omega \to \omega + i\eta$, the critical values determined by the two methods would be

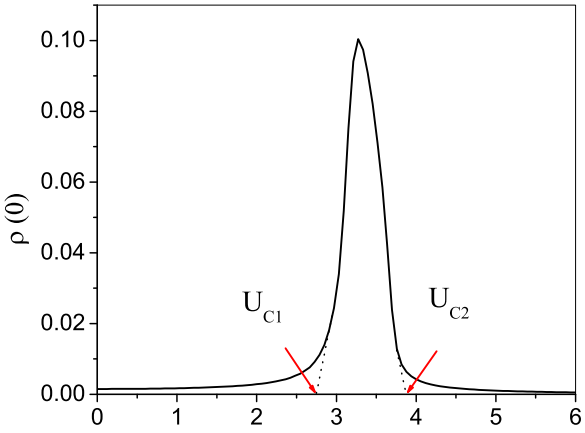

Fig. 3. The density of states at the Fermi level as a function of the onsite Coulomb repulsion. The critical values obtained by extrapolating $3.0t < U < 3.7t$ data is also indicated (t=1, λ=0.2).

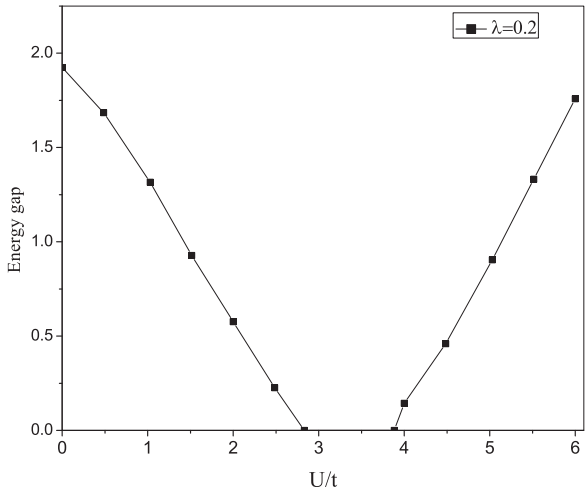

Fig. 4. The insulating gap as a function of the onsite Coulomb repulsion. The critical values obtained by extrapolating $U > 4.0t$ and $U < 2.5t$ data is also indicated (t=1, λ=0.2).

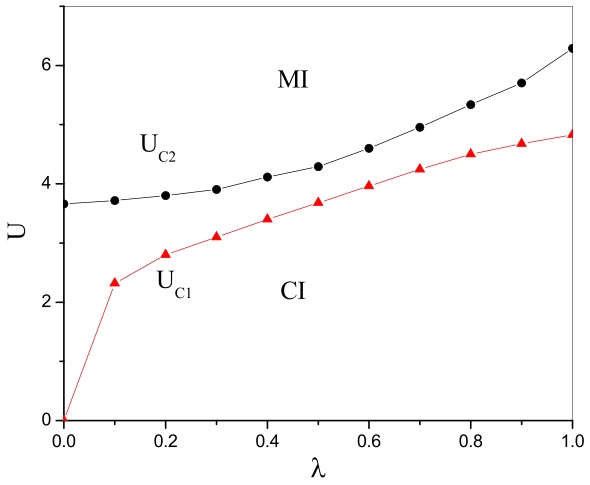

Fig. 5. The phase diagram at half filling, where CI denotes the Chern insulating phase, and MI denotes the Mott-insulating phase. The metallic phase exists between the CI and MI phases.

the same. Unlike the first method, the second one is not very sensitive with the choice of η because the imaginary part of the self-energy in the insulating phase is quite large. In order to construct the phase diagram, we will use critical values U_{C1} and U_{C2} calculated by the second method.

Next we analyze the topological properties of the two obtained insulating phases for small and large values of U. Because when U=0 the system is a Chern insulator, and the region of small values of U adiabatically connects with U=0, one can expect that the first insulating phase is a Chern insulator. In this region, the DOS clearly shows two separated subbands with an energy gap in between. The separation of two subbands increases with increasing U. However, the energy gap, decreases with increasing U. While electron correlations force the two subbands to separate, they actually also reduce the energy gap of the Chern insulator. At the critical value U_{C1} the gap closes, and the system turns into metallic phase. We will verify the topology of the first insulating phase by calculating directly the Chern number C, that is calculated via the Green's function at zero frequency [23,24]

$$C = \frac{1}{2\pi}\sum_{\sigma}\sigma\int d^2k\mathcal{F}_{\sigma xy}, \tag{7}$$

where $\mathcal{F}_{\sigma ij} = \partial_i\mathcal{A}_{\sigma j} - \partial_j\mathcal{A}_{\sigma i}$, $\mathcal{A}_{\sigma i} = -i\sum'_{\nu}\langle\vec{k}\,\sigma\nu|\partial_{k_i}|\vec{k}\,\sigma\nu\rangle$, and the sum is taken over all orthonormalized eigenstates $|\vec{k}\,\sigma\nu\rangle$ of matrix

$$\hat{G}^{-1}(\vec{k}\,\sigma, i0) = \begin{pmatrix} -\lambda\xi_{\vec{k}} - \Sigma_{A\sigma}(i0^+) & -t\gamma_{\vec{k}} \\ -t\gamma^{*}_{\vec{k}} & \lambda\xi_{\vec{k}} - \Sigma_{B\sigma}(i0^+) \end{pmatrix}, \tag{8}$$

with positive eigenvalues. In numerical calculations we use the efficient method of discretization of the Brillouin zone to calculate the Chern number in Eq. (7) [25]. Indeed, we obtain the Chern number C=2 when $U < U_{C1}$. The first insulator-metal transition is also the topological phase transition. The gap closes at the same point where the Chern number stops to be quantized. The metallic phase, where the DOS is finite at the Fermi energy, occurs for U ran from U_{C1} up to U_{C2}. At U_{C2} the gap opens again. For large values of U, the DOS also shows two separated subbands with an energy gap in between. The separation of two subbands as well as the energy gap increase with increasing U. We obtained that the system is in the Mott state with the Chern number C=0. The second insulator-metal transition is not topological phase transition.

By performing the same procedure for other values of λ, the full phase diagram of the system has been obtained within the CPA and it is shown in Fig. 5. It is obtained that the for small U the system is topological band insulator whereas for large U the system is topologically trivial Mott insulator. That result is in good agreement with the calculation of the Haldane-Falicov-Kimball model within the dynamical mean-field theory (DMFT) [17]. However, we do not find the charge ordered states at low temperatures. This is the known discrepancy between the Hubbard and the Falicov-Kimball models. Also, we do not find the antiferromagnetic state for large U as reported in [15,16]. For intermediate values of the local interaction, $U_{C1} < U < U_{C2}$ we found a metallic state as in [17] that differs with what found by strong U approach [15,16]. The Hamiltonian (1) under consideration breaks time-reversal symmetry, which leads to the notorious fermion sign problem and precludes the use of methods based on the quantum Monte-Carlo algorithm. Therefore, at the moment, the exact answer to the phase in the intermediate U region is not available. Our results serve as a complementary information for future study.

4. Conclusions

We have applied the coherent potential approximation to study a two-dimensional Haldane-Hubbard model on a honeycomb lattice. Our calculated critical values are indeed in good agreement with results in the Haldane-Falicov-Kimball model within the DMFT [17]. The study here is restricted for small and intermediate value of the local interaction U and can be extended to take in to account the ionic potential that described the effects of the ionic potential induced by the Ag substrate on silicene. With the introduction of the ionic potential, the system loses its Dirac fermion characteristics with the effect of the substrate as a consequence of the symmetry breaking induced by a charge density wave [6,12,13]. In this case, the problem becomes more realistic but at the same time more complex and thus goes beyond the scope of the present paper. We leave this problem for future study.

Acknowledgments

This research is funded by Vietnam National Foundation for Science and Technology Development (NAFOSTED) under grant number 103.01-2015.21

References

[1] K.S. Novoselov, et al., Science 306 (2004) 666;
K.S. Novoselov, et al., Nature 438 (2005) 197.
[2] P. Vogt, et al., Phys. Rev. Lett. 108 (2012) 155501.
[3] Abdelkader Kara, et al., Surf. Sci. Rep. 67 (2012) 1–18.
[4] L. Tao, et al., Nat. Nanotechnol. 10 (2015) 227.
[5] B. Lalmi, et al., Appl. Phys. Lett. 97 (2010) 223109.
[6] D.A. Rowlands, Zhang Yu-Zhong, Chin. Phys. B 23 (2014) 037101.

[7] F.D.M. Haldane, Phys. Rev. Lett. 61 (1988) 2015.
[8] W. Zheng, H. Zhai, Phys. Rev. A 89 (2014) 061603.
[9] G. Jotzu, et al., Nature 515 (2014) 237.
[10] S. Raghu, et al., Phys. Rev. Lett. 100 (2008) 156401.
[11] C.N. Varney, et al., Phys. Rev. B 84 (2011) 241105 (R).
[12] T.I. Vanhala, et al., Phys. Rev. Lett. 116 (2016) 225305.
[13] J. Imriška, et al., Phys. Rev. B 94 (2016) 035109.
[14] C. Hickey, et al., Phys. Rev. B 91 (2015) 134414.
[15] V.S. Arun, et al., Phys. Rev. B 93 (2016) 115110.
[16] J. Wu, et al., Phys. Rev. B 93 (2016) 075131.
[17] H.S. Nguyen, M.T. Tran, Phys. Rev. B 88 (2013) 165132.
[18] D.A. Le, Mod. Phys. Lett. B 27 (2013) 1350046.
[19] J. He, et al., Phys. Rev. B 85 (2011) 035127.
[20] X.-J. Liu, et al., New J. Phys. 18 (2016) 035004.
[21] W. Zheng, et al., Phys. Rev. B 91 (2015) 161107.
[22] Y.-J. Wu, et al., Eur. Phys. J. B 88 (2015) 255.
[23] V. Gurarie, Phys. Rev. B 83 (2011) 085426.
[24] Z. Wang, S.-C. Zhang, Phys. Rev. X 2 (2012) 031008.
[25] T. Fukui, et al., J. Phys. Soc. Jpn. 74 (2005) 1674.